Archives of Materials Science and Engineering

Volume 41
Issue 2
February 2010
Pages 77-84

International Scientific Journal
published monthly by the
World Academy of Materials
and Manufacturing Engineering

Corrosion resistance of high-manganese austenitic steels

A. Grajcar*, S. Kołodziej, W. Krukiewicz
Division of Constructional and Special Materials, Institute of Engineering Materials and Biomaterials, Silesian University of Technology,
ul. Konarskiego 18a, 44-100 Gliwice, Poland
* Corresponding author: E-mail address: adam.grajcar@polsl.pl

Received 10.12.2009; published in revised form 01.02.2010

ABSTRACT

Purpose: The aim of the paper is to compare the corrosion resistance of two new-developed high-manganese austenitic steels in 1N H_2SO_4 and 3.5% NaCl solutions.

Design/methodology/approach: The steels used for the investigation were thermo-mechanically rolled and then solution heat-treated from a temperature of 850°C. Corrosion resistance of investigated steels was examined using the immersion test. The specimens were weighed and dipped in the prepared solutions for 100 h. After the test, the percentage weight loss was calculated. The metallographic investigations of corrosion damages included light and scanning electron microscope observations both in the polished and etched states.

Findings: It was found that after the thermo-mechanical processing one steel is characterized by an austenitic structure with numerous annealing twins, whereas in the second steel ε and α' martensite plates in an austenitic matrix were observed. According to the results of the immersion tests it was found that the examined steels exhibit a comparable corrosion resistance. They show very poor corrosion resistance in H_2SO_4 solution and low corrosion resistance in NaCl medium. The weight loss in chloride solution is much lower, what is explained by different corrosion mechanisms. In both the solutions, the intensive general corrosion and corrosion pitting were observed. In acidic medium they are created in a way of hydrogen depolarization and in NaCl in the way of oxygen depolarization.

Research limitations/implications: To investigate in more detail the corrosion behaviour of high-manganese austenitic steels, the investigations should include polarization tests and an analysis of corrosion products.

Practical implications: The obtained results can be used to search for the appropriate way of improving the corrosion resistance of high-manganese steels with a single-phase austenitic structure as well as the austenite structure containing ε and α' martensite.

Originality/value: The corrosion resistance of two types of advanced high-strength high-manganese austenitic steels with different initial structures was compared in acidic and chloride solutions.

Keywords: Corrosion resistance; High-manganese steels; TWIP-effect; Immersion test; General corrosion; Corrosion pits

Reference to this paper should be given in the following way:

A. Grajcar, S. Kołodziej, W. Krukiewicz, Corrosion resistance of high-manganese austenitic steels, Archives of Materials Science and Engineering 41/2 (2010) 77-84.

PROPERTIES

1. Introduction

High-manganese austenitic steels belong to the second generation of modern high strength steels for automotive industry [1]. Their mean advantage over first generation steels with a matrix based on A2 lattice structure [2-4] is the great susceptibility of austenite on plastic deformation, during which dislocation glide, mechanical twinning, and strain-induced martensitic transformation can occur. The group of high-manganese steels includes alloys with 15-30% manganese content. Two mean conceptions of chemical composition projecting had been worked out so far. The first includes alloys with different Mn concentration and 0.5 to 0.8% carbon content [5, 6]. The function of carbon is stabilization of γ phase – the same as Mn – and hardening of solid solution. In the second group, the concentration of carbon is decreased to about 0.1%, whereby there is an addition up to 4% Al and/or 4% Si [7-9]. The solid solution strengthening caused by the presence of Al and Si compensates smaller carbon concentration. Moreover these elements have an impact on SFE (Stacking Fault Energy) of austenite, deciding which mechanism of steel deformation will be dominant. Silicon – same as Mn up to about 15% content – decreases SFE, whereas aluminium has an inversely effect, foster austenite stabilization.

Mechanical properties of these steels depend on structural processes occurring during cold plastic deformation, which are highly dependent on SFE of austenite [6-9]. If it is from 12 to 20 mJm^{-2}, a partial transformation of austenite into martensite occurs, taking advantage of TRIP (TRansformation Induced Plasticity) effect [7-10]. Values of SFE equal from 20 to 60 mJm^{-2} determine intense course of mechanical twinning connected to TWIP effect (TWinning Induced Plasticity) [5-9]. High impact on the dominating deformation mechanism has also the temperature and strain rate [7, 8, 11]. Making use of these phenomena allows achieving mechanical properties of steels in a wide range, i.e. $YS_{0.2}$ = 250-400 MPa, UTS = 500-1000 MPa, UEl = 30-70%. This beneficial connection of mechanical properties predisposes described steels for their application for parts with high energy absorption requirements, as well as for parts with complicated shape.

Up to now the mean area of studies on high manganese steels was their high-temperature deformation resistance [5, 12-15] and especially cold-working behaviour [6-11]. There are a few reports available on the corrosion behaviour of these steels [16-20]. Zhang and Zhu [16] reported that addition of 25% Mn to mild steel was very detrimental to the corrosion resistance in aqueous solutions. The Fe-25Mn alloy was difficult to passivate, even in such neutral aqueous electrolytes as 1M Na_2SO_4 solution. The other alloying elements can alter the corrosion behaviour due to the differences in their electrochemical properties [17]. It is well known, that owing to its high passivity, aluminium enhances the corrosion resistance, whereas the influence of silicon is inversely [21]. Zhang and Zhu [16] further reported that with increasing Al content up to 5% of the Fe-25Mn-Al steel, the anodic polarization curves exhibit a stable passivation region in Na_2SO_4 solution, but it shows still no passivation in 3.5% NaCl solution. The corrosion behaviour of Fe-C-Mn-Al steels was confirmed by Altstetter et. al. [20], who worked on investigation of substitutes for expensive Cr-Ni steels for cryogenic applications. The role of manganese boils to Ni replacement and obtaining austenitic microstructure, whereas aluminium has a similar impact as chromium. Improvement of corrosion resistance by Al consists in formation of thin, stable layer of oxides. They found that Fe-C-Mn-Al steels show inferior corrosion resistance than Cr-Ni steels and they can be used as a substitute only in some applications [20].

Recently, corrosion resistance of Fe-0.05C-29Mn-3.1Al-1.4Si steel in acidic (0.1M H_2SO_4) and chloride-containing (3.5% NaCl) environments was investigated by Kannan et. al. [17]. Moreover, they compared the corrosion behaviour of the tested steel with that of IF-type (Interstitial-Free) steel. Performing immersion and polarization tests they found [17], that Fe-Mn-Al-Si steel has lower corrosion resistance than IF steel, both in acidic and in chloride media. However, the corrosion resistance of the high-manganese steel in chloride solutions is higher compared to that observed in acidic medium. Recently corrosion tests for steels with similar chemical compositions (excluding carbon content) in 3.5% NaCl solution were also made by Ghayad et. al. [18]. They found that Fe-0.5C-29Mn-3.5Al-0.5Si steel shows no passivation, independently on the state of the heat treatment: supersaturated, aged or strain-aged. The steel corroded, particularly intensively in the presence of some ferrite fraction, formed during ageing. Faster corrosion progress is a result of creation of a galvanic couple between ferrite and an austenitic matrix. They further reported that cold working increases corrosion rate because of deformation twins, which represent regions of different potential from the matrix and this led to the increase in the corrosion current density [18].

The behaviour of Fe-0.2C-25Mn-(1-8)Al steels with increased concentration of Al up to 8% wt. in 3.5% NaCl was investigated by Hamada [19]. He reported that the corrosion resistance of tested steels in chloride environments is pretty low. The predominating corrosion type is the general corrosion, but locally corrosion pits were observed. In steels including up to 6% Al with homogeneous austenite structure, places where the pits occur are casually, whereas in case of two-phase structure, including ferrite and austenite (Fe-0.2C-25Mn-8Al), they preferentially occur in α phase. Hamada et. al. [22] showed that corrosion resistance of examined steels can be increased trough anodic passivation in nitric acid, which provides modification of chemical composition and constitution of the surface layer. This was done by reducing the surface concentration of Mn and enriching the surface layer in elements that improve the corrosion resistance (e.g. Al, Cr). A better effect in corrosion resistance increasing was reached by chemical composition modification. It was found [19] that addition of Al and Cr to Fe-0.26C-30Mn-4Al-4Cr and Fe-0.25C-30Mn-8Al-6Cr steels increases considerably the general corrosion resistance, especially after anodic passivation ageing of surface layers in an oxidizing electrolytic solution. Cr-bearing steels passivated by nucleation and growth of the passive oxide films on the steel surface, where the enrichment of Al and Cr and depletion of Fe and Mn have occurred [19].

Studies on high-manganese steels corrosion behaviour are confined to following alloy types: Fe-Mn, Fe-Mn-Al and Fe-Mn-Al-Cr. There are no results concerning steels with increased silicon content. Realized structural examinations of Fe-0.05-25Mn-3.5Si-1.6Al-Ti-Nb steel [13] showed, besides the austenitic matrix, some fraction of martensite ε. The presence of martensite is a result of a decrease of austenite SFE, reached by adding Si and also, to some extent, Ti and Nb, which are fixing carbon and nitrogen, resulting

with a decrease of γ phase stability. The presence of a second phase with a lamellar shape can have great impact on corrosion processes, same as the presence of ferrite in the austenite matrix [18, 19]. Results of initial corrosion resistance tests in 0.5N NaCl, using the potentiodynamic method, has shown [23], that Fe-Mn-Si-Al-type steel exhibits low corrosion resistance, due to the intensive general and pitting corrosion.

2. Experimental procedure

Examinations were carried out on two high-manganese steels with chemical composition presented in Table 1. The steels were vacuum melted in the Institute for Ferrous Metallurgy in Gliwice. Investigated steels have similar C and Mn content. Significant impact on the stacking fault energy (SFE) of austenite has the difference in Al, Si and Ti concentration. On lower SFE of 24.5Mn-3.5Si-1.5Al-Nb-Ti steel than that of 26Mn-3Si-3Al-Nb-Ti steel, higher silicon and lower aluminium concentrations have impact. Moreover, much larger titanium content provides a decrease of γ phase stability, as a result of fixing the total nitrogen and a part of carbon [13].

Table 1.
Chemical composition of the investigated steels

Component	Mass contents, (%)	
	26Mn-3Si-3Al-Nb-Ti	24.5Mn-3.5Si-1.5Al-Nb-Ti
C	0.065	0.054
Mn	26.0	24.4
Si	3.08	3.49
Al	2.87	1.64
P	0.004	0.004
S	0.013	0.016
Nb	0.034	0.029
Ti	0.009	0.075
N	0.0028	0.0039
O	0.0006	0.0006
Initial structure		
	γ	γ+ε+α’

The steels were examined in a state after the thermo-mechanical treatment, with parameters described in [23]. Taking into account the high deformation resistance during hot-working [13, 14], the amounts of deformation during rolling were equal from 25 to 15%. In these conditions, the process to control the work hardening during the last rolling pass at a temperature of 850°C was the dynamic recovery. After finished rolling, the steel sheets were held at a temperature of 850°C for 15 seconds, and next supersaturated in water. The steel structures after the thermo-mechanical treatment are shown in Figs. 1 and 2. The 26Mn-3Si-3Al-Nb-Ti steel exhibits a homogeneous austenite structure with grains elongated in the rolling direction (Fig. 1a). The susceptibility to twinning confirms the presence of a great number of annealing twins. The single-phase structure of the steel is revealed by X-ray diffraction pattern in Fig. 1b. The lower stacking fault energy of the 24.5Mn-3.5Si-1.5Al-Nb-Ti steel results in the presence of the second phase with a lamellar shape, distributed in the austenite matrix (Fig. 2a). The number of annealing twins is lower. Moreover, non-metallic inclusions are present. The X-ray diffraction analysis confirms the presence of ε martensite (Fig. 2b), like in the state after initial forging of the ingots [13]. Moreover, a peak of martensite α’ was identified, indicating low stacking fault energy of the steel. Martensite α’ has also a lamellar shape and its unequivocal distinction from lamellas of ε phase is complicated. Usually, privileged places for martensite α’ forming are crossings of ε martensite lamellas [24]. This matter will be the topic of future studies.

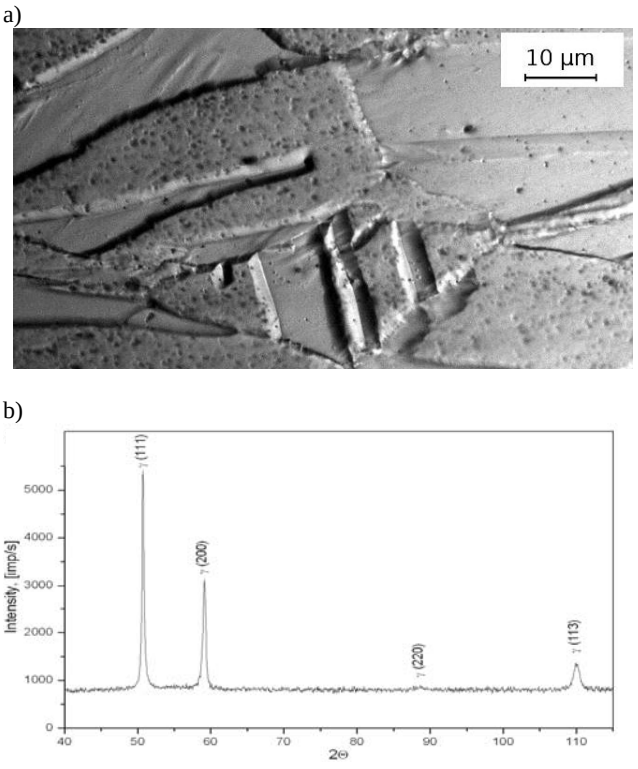

Fig. 1. Austenitic structure with annealing twins of 26Mn-3Si-3Al-Nb-Ti steel in the initial state (a) and X-ray diffraction pattern (b)

The corrosion resistance of the investigated steels was assessed using immersion tests in two solutions: 1N H_2SO_4 and 3.5% NaCl. Prior to the corrosion tests, three samples of the each steel with the size 3.2x10x15 mm were ground to the 1000-grit finish and then they were washed in distilled water, ultrasonically cleaned in acetone and finally rinsed with ethanol and dried. The specimens were weighed with the accuracy of 0.001g and put into the solution for 100 hours. The temperature of the test was equal 23±1°C. After the test the specimens were weighed and analysed using light and scanning electron microscopes. Corrosion loss was calculated in a simple way:

$$m_d = m_i - m_f \quad (1)$$

where: m_d – mass decrement [g], m_i – initial mass [g], m_d – final mass [g].

Percentage mass decrement (m_p) was determined as follows:

$$m_p = \frac{m_d}{m_i} \cdot 100\% \quad (2)$$

a)

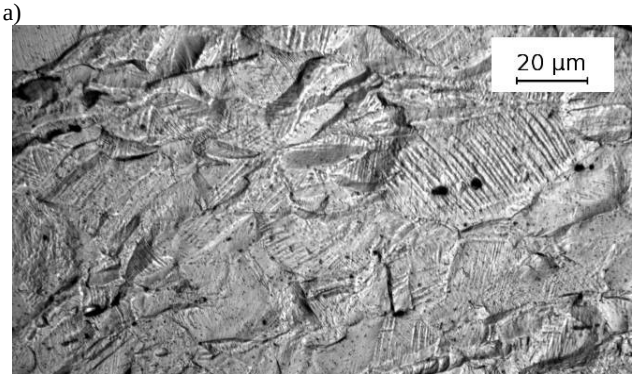

b)

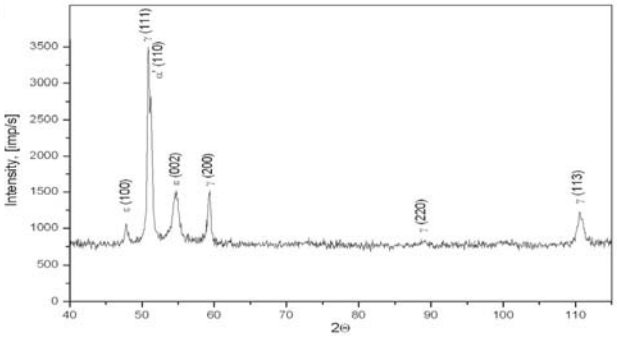

Fig. 2. Austenitic matrix containing ε and α' martensite plates, annealing twins and non-metallic inclusions of 24.5Mn-3.5Si-1.5Al-Nb-Ti steel in the initial state (a) and X-ray diffraction pattern (b)

Microstructure observations of the specimens etched in nital were carried out on LEICA MEF 4A light microscope, with magnifications from 100 to 1000x. Fractographic investigations were carried on a scanning electron microscope SUPRA 25 (Zeiss) at the accelerating voltage of 20kV. In order to remove corrosion products, the specimens were ultrasonically cleaned before the analysis.

In order to recognize the phase structure of steels, the X-ray phase analysis was also carried out (Figs. 1b, 2b) using the X'Pert PRO diffractometer with the X'Celerator detector. The presence of martensite ε in the steel structure was additionally exhibited by microhardness measurements on the PMT-3 device, using the Vickers method by load equal 0.49N.

3. Results

Metallographic investigations and microhardness test results (Table 2) confirmed a diversified phase structure of investigated steels. The obtained microhardness values are among 250 and 450 HV0.05. The average microhardness of austenite for 26Mn-3Si-3Al-Nb-Ti steel is 267 HV0.05 and for 24.5Mn-3.5Si-1.5Al-Nb-Ti steel: 284 HV0.05. Hardness of lamellar areas in the steel with ε and α' martensites are among 347 and 423 HV0.05, whereby the highest values are induced by the presence of α' phase. The structures shown in Figs. 3 and 4 do not include fine recrystallized grains, similarly to structures in Figs. 1 and 2, what bears that after rolling at 850°C the static recrystallization didn't take place.

Table 2.
HV0.05 microhardness range for individual microstructural constituents

	26Mn-3Si-3Al-Nb-Ti	24.5Mn-3.5Si-1.5Al-
γ_{matrix}	245-298	263-312
$\varepsilon(\alpha')_{martensite}$	-	347-423

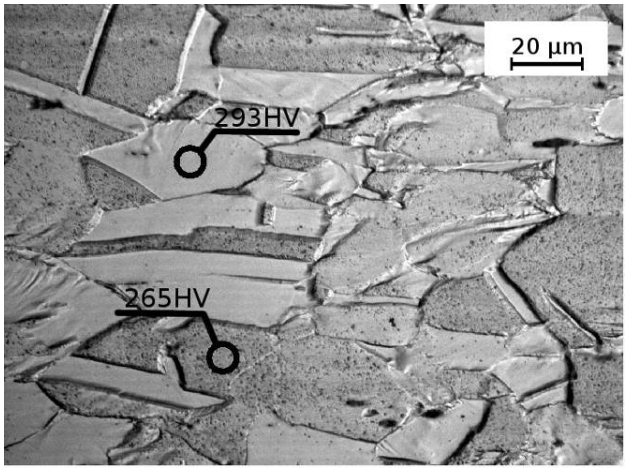

Fig. 3. Austenitic structure with many annealing twins and microhardness test results of 26Mn-3Si-3Al-Nb-Ti steel

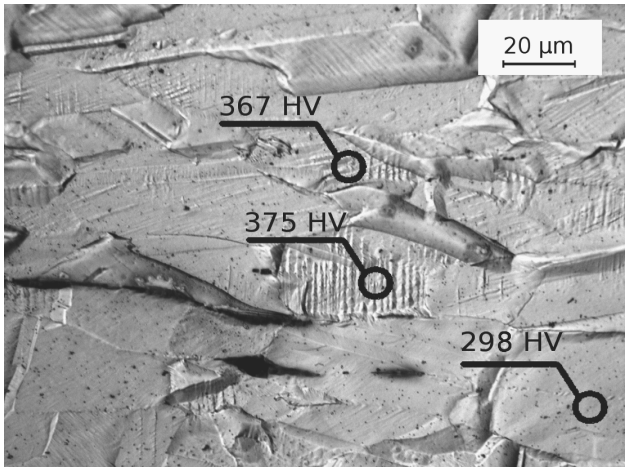

Fig. 4. Austenitic matrix containing ε and α' martensite plates and microhardness test results of 24.5Mn-3.5Si-1.5Al-Nb-Ti steel

The results of the immersion tests in two media and the calculated mean percentage mass loss are listed in Tables 3 and 4, respectively.

Table 3.
Results of the immersion test

1N H_2SO_4					
26Mn-3Si-3Al-Nb-Ti			24.5Mn-3.5Si-1.5Al-Nb-Ti		
m_i, g	m_f, g	m_d, g	m_i, g	m_f, g	m_d, g
3.34	2.29	1.05	3.68	2.59	1.09
3.23	2.02	1.21	3.84	2.36	1.48
3.52	1.89	1.63	3.75	1.66	2.09
3.5% NaCl					
26Mn-3Si-3Al-Nb-Ti			24.5Mn-3.5Si-1.5Al-Nb-Ti		
m_i, g	m_f, g	m_d, g	m_i, g	m_f, g	m_d, g
2.452	2.441	0.011	3.417	3.401	0.016
3.207	3.194	0.013	3.572	3.553	0.019
2.864	2.854	0.010	3.189	3.175	0.014

Table 4.
Mean percentage mass decrement after the corrosion tests, %

1N H_2SO_4	
26Mn-3Si-3Al-Nb-Ti	24.5Mn-3.5Si-1.5Al-Nb-Ti
38.4±5.2	41.3±9.6
3.5% NaCl	
26Mn-3Si-3Al-Nb-Ti	24.5Mn-3.5Si-1.5Al-Nb-Ti
0.401±0.035	0.480±0.035

After 100 hours immersion in 1N H_2SO_4 both steels showed a significant percentage mass decrement, among 38 and 41% (Table 4). Mass decrement of specimens dipped in 3.5% NaCl is about 100 times lower. The difference is due to different corrosion mechanisms. When the solution is acidic, the corrosion process is running according to hydrogen depolarization, whereas in chloride media the specimens are corroding with oxygen depolarization.

In 26Mn-3Si-3Al-Nb-Ti steel dipped in 1N H_2SO_4 many deep corrosion pits along the whole specimen surface were observed (Fig. 5). Moreover, in places with higher density of non-metallic inclusions, microcracks locally occur. Similar pits are present in the steel with lower aluminum content (Fig. 6). Slightly smaller corrosion pits are formed in specimens after the immersion test in 3.5% NaCl, regardless of a steel type (Fig. 7). Places privileged to creation of corrosion pits are pointwise aggregations and chains of non-metallic inclusions.

Characteristically for the structure of 24.5Mn-3.5Si-1.5Al-Nb-Ti steel dipped in 3.5% NaCl solution are small microcracks located along the ε martensite (relatively α') lamellas. It is possible to observe in Fig. 4, that they are propagated from significantly elongated in a rolling direction, sulphuric non-metallic inclusions. In specimens with single-phase austenitic structure, microcracks were not observed.

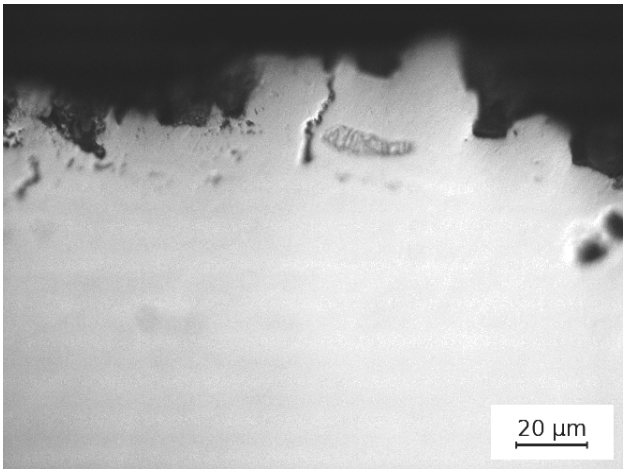

Fig. 5. Corrosion pits and microcracks in 26Mn-3Si-3Al-Nb-Ti steel after the immersion test in 1N H_2SO_4

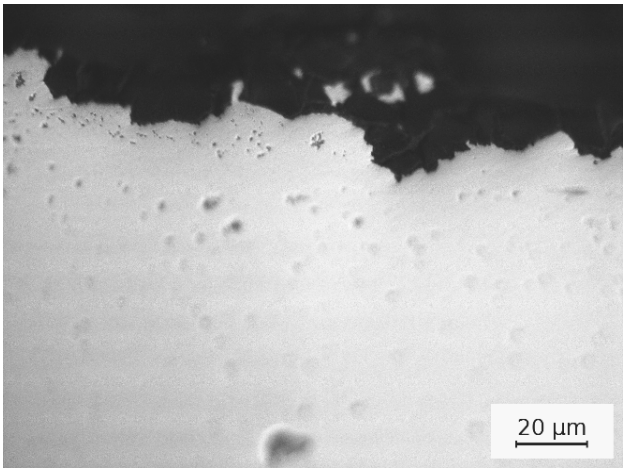

Fig. 6. Corrosion pits in 24.5Mn-3.5Si-1.5Al-Nb-Ti steel after the immersion test in 1N H_2SO_4

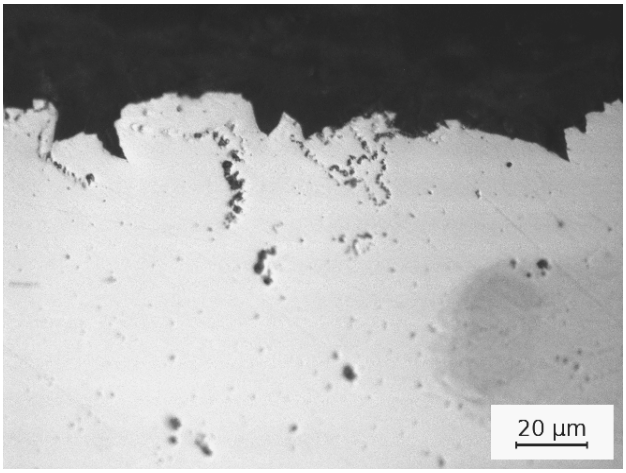

Fig. 7. Corrosion pits in 24.5Mn-3.5Si-1.5Al-Nb-Ti steel after the immersion test in 3.5% NaCl

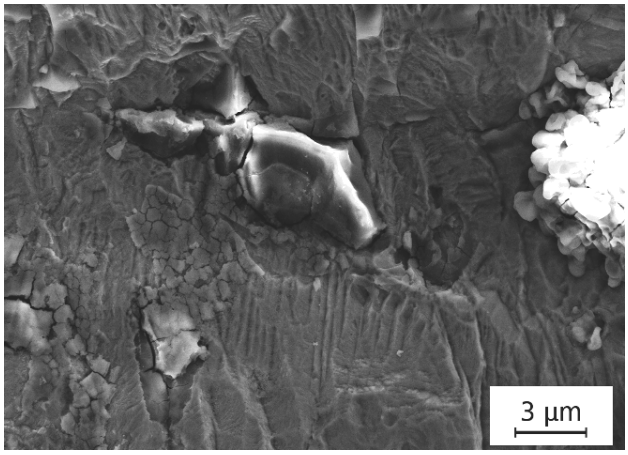

Fig. 8. Bursted corrosion products layer on 26Mn-3Si-3Al-Nb-Ti steel surface after the immersion test in 3.5% NaCl

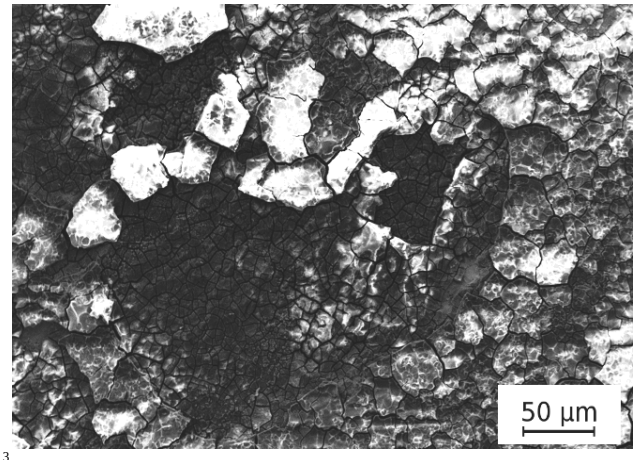

3

Fig. 9. Craters created as a result of hydrogen desorption and bursted corrosion products layer in 24.5Mn-3.5Si-1.5Al-Nb-Ti steel after the immersion test in 1N H_2SO_4

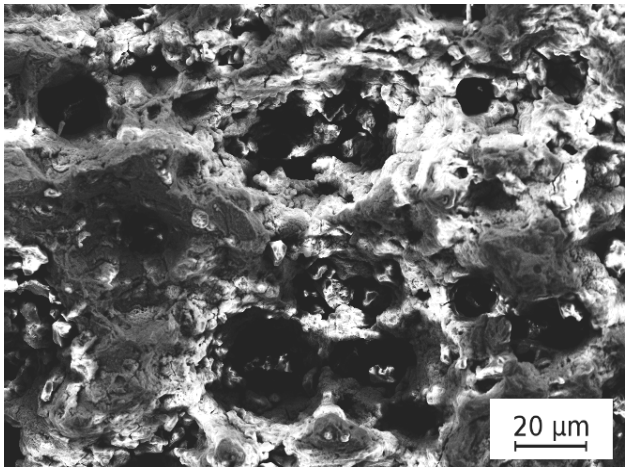

Fig. 10. Craters created as a result of hydrogen desorption and corrosion products residues in 26Mn-3Si-3Al-Nb-Ti steel after the immersion test in 1N H_2SO_4

4. Discussion

The test results confirmed the low corrosion resistance of high-manganese steels in acidic and chloride media. Especially low corrosion resistance the investigated steels show in 1N H_2SO_4, where the mass decrement is about 40%, what is about 100 times higher than for specimens dipped in 3.5% NaCl (Tables 3 and 4). The similar order of magnitude of corrosion progress was observed by Kannan et. al. [17] for Fe-0.05C-30Mn-3Al-1.4Si steel. Convergent with immersion tests were the results of polarization experiments, where was shown [17], that the corrosion current values in acidic solution are more than 2 orders of magnitude higher than that in chloride solution. The high corrosion resistance difference is a case of different corrosion mechanisms in both environments.

The big mass loss in the H_2SO_4 solution is due to the hydrogen depolarization mechanism, which is typical for corrosion in acidic media. Hydrogen depolarization is a process of reducing hydrogen ions (from the electrolyte) in cathodic areas by electrons from the metal, to gaseous hydrogen, resulting in continuous flow of electrons outer the metal and consequently the corrosion progress [24]. Due to this process, numerous corrosion pits occur in examined steels (Figs. 5, 6). Corrosion pits are occurring most intensively in places with high density of non-metallic inclusions. They are less precious than the rest of material, fostering potential differences and galvanic cell creation. This causes the absorption of hydrogen ions, which, due to increasing pressure and temperature, recombine to a gaseous form and get out of the metal creating characteristic craters (Fig. 10). This process is accompanied by local cracking of corrosion products layer (Figs. 9, 10), uncovering the metal surface and causing further penetration of the corrosion medium and the intensive corrosion progress [24].

In chloride solution, the corrosion process is running according to the oxygen depolarization, like in all neutral and basic solutions. In this mechanism, oxygen included in the electrolyte is being reduced by electrons from the metal to hydroxide ions [24]. On the surface of the alloy appears a layer of corrosion products (Fig. 8), protecting the material before further penetration of the corrosion medium. This is why the mass loss in chloride solution is much lower compared to acidic medium. At less corrosion-resistant places (e.g. with non-metallic inclusions) potential differences are occurring. This enables the absorption of chloride ions, which are forming chlorine oxides of increased solubility [24]. This results in local destructions of corrosion products layer (Fig. 8) and the initiation of corrosion pits (Fig. 7). Further pit expansion is running autocatalytic.

As a consequence of small steel softening during static recrystallization (Figs. 1-4), after finished rolling, the state of internal stresses in examined steels can be increased. In specimen areas with internal stresses, crevices are occurring. Due to limited oxygen access and a lack of possibility of corrosion products layer forming, they become susceptible to corrosion. As a result of chloride ions adsorption on the crevice bottom, a concentrated electrolyte solution is forming, fostering the corrosion progress [25]. As a result, stress corrosion cracking takes place. Microcracks were observed along ε martensite lamellas in 24.5Mn-3.5Si-1.5Al-Nb-Ti steel. The microcracks initiation proceeds in places with elongated non-metallic inclusions (Fig. 4),

while their propagation runs along lamellar precipitations of the second phase with much higher hardness than the hardness of the austenitic matrix (Table 2). In the steel with a single-phase austenitic structure, microcracks were not observed.

The mass decrement in both steels is comparable (Table 4) in acidic and chloride media. It indicates that a small ε(α') martensite fraction doesn't have meaningful impact on the corrosion progress. The observed corrosion products are related rather to the chemical composition than to the phase structure of investigated steels. That confirms a slightly higher mass decrement in the steel with lower aluminium and somewhat higher silicon content. In general, the low corrosion resistance of high-manganese steels is coming from the fact, that manganese in steels forms unstable manganese oxide due to low passivity coefficient and hence reduces their electrochemical corrosion resistance [17]. It provides consequently to the high dissolution rate of manganese and iron atoms both in H_2SO_4 and NaCl solutions [16-19].

The high mass decrement of steels examined in H_2SO_4 solution is a result of fast general corrosion progress and corrosion pits formation (Figs. 5, 6, 9). Much lower mass decrement in steels examined in NaCl solution (Tables 3 and 4) is connected with corrosion pits forming only (Fig. 7). The presence of corrosion pits in chloride medium in steels of the type Fe-25Mn-5Al and Fe-0.2C-25Mn-(1-8)Al was confirmed by Zhang and Zhu [16] and Hamada [19]. Localized corrosion attack in the investigated steels is enhanced by the lower aluminium and higher silicon concentrations. Significant participation of pitting corrosion was not observed by Kannan et al. [17] in studies on Fe-0.05C-29Mn-3.1Al-1.4Si steel and Ghayad et. al. [18] on Fe-0.5C-29Mn-3.5Al-0.5Si steel. It means that a character of corrosion damages in high-manganese steels in chloride media is a complex reaction of the chemical composition and structural state related with a phase composition and the degree of strain hardening. Moreover, the results discrepancies could be a consequence of some differences in corrosion test conditions and a preparation of the specimen surface. These matters and especially the role of Nb and Ti will be discussed in a further research.

5. Conclusions

The worked out investigations have showed, that both examined steels, independent of initial structure, have a very low corrosion resistance in acidic medium and a low corrosion resistance in chloride solution. In particular it was found that:

- the mass decrement of specimens immersed in 1N H_2SO_4 for 100 hours is equal about 40% and is about 100 higher compared to the specimens immersed in 3.5% NaCl;
- the percentage mass decrement in steel with single-phase austenitic structure is slightly lower than in steel with martensite lamellas. However, any significant impact of the second phase on corrosion process acceleration was not observed;
- the decisive impact on the corrosion resistance of examined steels has their chemical composition, which determines the high speed of manganese and iron dissolution in acidic solution. The oxygen depolarization process decides on corrosion products layer formation on the surface of the steel examined in chloride medium. Therefore, the mass decrement of steels in 3.5% NaCl is much lower than in 1N H_2SO_4;
- a higher mass decrement of 24.5Mn-3.5Si-1.5Al-Nb-Ti steel is a result of the lower aluminium content and probably higher silicon content than in 26Mn-3Si-3Al-Nb-Ti steel;
- both steels are liable to general and pitting corrosion, especially intensively in the sulphuric acid solution. A very adverse influence on corrosion pitting initiation has a relative large fraction of non-metallic inclusions, especially of that forming local aggregations. In chloride solution it also results in occurring local microcracks, nucleating at elongated non-metallic inclusions and growing along hard martensite lamellas;
- the surface layer of corrosion products has many cracks, especially in surroundings of corrosion pits and non-metallic inclusions. In case of acidic solution, the cracks are also formed round craters created due to hydrogen desorption.

References

[1] D. Matlock, Microstructural aspects of advanced high strength sheet steels, Report of Advanced High Strength Steels Workshop, Arlington, Virginia, 2006, 1-25.

[2] R. Kuziak, R. Kawalla, S. Waengler, Advanced high strength steels for automotive industry, Archives of Civil and Mechanical Engineering 8/2 (2008) 103-117.

[3] J. Adamczyk, A. Grajcar, Heat treatment and mechanical properties of low-carbon steel with dual-phase microstructure, Journal of Achievements in Materials and Manufacturing Engineering 22/1 (2007) 13-20.

[4] A. Grajcar, Hot-working in the γ+α region of TRIP-aided microalloyed steel, Archives of Materials Science and Engineering 28/12 (2007) 743-750.

[5] B. Wietbrock, M. Bambach, S. Seuren, G. Hirt, Homogenization strategy and material characterization of high-manganese TRIP and TWIP steels, Materials Science Forum 638-642 (2010) 3134-3139.

[6] J.A. Jimenez, G. Frommeyer, Microstructure and texture evolution in a high manganese austenitic steel during tensile test, Materials Science Forum 638-642 (2010) 3272-3277.

[7] G. Frommeyer, U. Brüx, P. Neumann, Supra-ductile and high-strength manganese-TRIP/TWIP steels for high energy absorption purposes, ISIJ International 43 (2003) 438-446.

[8] O. Grässel, L. Krüger, G. Frommeyer, L.W. Meyer, High strength Fe-Mn-(Al, Si) TRIP/TWIP steels development – properties – application, International Journal of Plasticity 16 (2000) 1391-1409.

[9] S. Allain S, J-P. Chateau, D. Dahmoun, O. Bouaziz, Modeling of mechanical twinning in a high manganese content austenitic steel, Materials Science and Engineering A 387-389 (2004) 272-277.

[10] B.X. Huang, X.D. Wang, Y.H. Rong, L. Wang, L. Jin, Mechanical behaviour and martensitic transformation of an Fe-Mn-Si-Al-Nb alloy, Materials Science and Engineering A 438-440 (2006) 306-313.

[11] T. Bator, Z. Muskalski, S. Wiewiórowska, J.W. Pilarczyk, Influence of the heat treatment on the mechanical properties and structure of TWIP steel in wires, Archives of Materials Science and Engineering 28/6 (2007) 337-340.
[12] L.A. Dobrzański, A. Grajcar, W. Borek, Influence of hot-working conditions on a structure of high-manganese austenitic steels, Journal of Achievements in Materials and Manufacturing Engineering 29/2 (2008) 139-142.
[13] A. Grajcar, M. Opiela, G. Fojt-Dymara, The influence of hot-working conditions on a structure of high-manganese steel, Archives of Civil and Mechanical Engineering 9/3 (2009) 49-58.
[14] L.A. Dobrzański, A. Grajcar, W. Borek, Hot-working behaviour of high-manganese austenitic steels, Journal of Achievements in Materials and Manufacturing Engineering 31/1 (2008) 7-14.
[15] L.A. Dobrzański, A. Grajcar, W. Borek, Microstructure evolution and phase composition of high-manganese austenitic steels, Journal of Achievements in Materials and Manufacturing Engineering 31/2 (2008) 218-225.
[16] Y.S. Zhang, X.M. Zhu, Electrochemical polarization and passive film analysis of austenitic Fe-Mn-Al steels in aqueous solutions, Corrosion Science 41 (1999) 1817-1833.
[17] M.B. Kannan, R.K.S. Raman, S. Khoddam, Comparative studies on the corrosion properties of a Fe-Mn-Al-Si steel and an interstitial-free steel, Corrosion Science 50 (2008) 2879-2884.
[18] I.M. Ghayad, A.S. Hamada, N.N. Girgis, W.A. Ghanem, Effect of cold working on the aging and corrosion behaviour of Fe-Mn-Al stainless steel, Steel Grips 4 (2006) 133-137.
[19] A.S. Hamada, Manufacturing, mechanical properties and corrosion behavioiur of high-Mn TWIP steels, Acta Universitatis Ouluensis C 281 (2007) 1-51.
[20] C.J. Altstetter, A.P. Bentley, J.W. Fourine, A.N. Kirkbridge, Processing and properties of Fe-Mn-Al alloys, Materials Science and Engineering A82 (1986) 13-25.
[21] H.J. Cleary, N.D. Greene, Corrosion properties of iron and steel, Corrosion Science 7 (1967) 821-831.
[22] A.S. Hamada, L.P. Karjalainen, M.A. El-Zeky, Effect of anodic passivation on the corrosion behaviour of Fe-Mn-Al steels in 3.5%NaCl, Proceedings of the 9th International Symposium "Passivation of Metals and Semiconductors and the Properties of Thin Oxide Layers", Paris, 2005, 77-82.
[23] M. Opiela, A. Grajcar, W. Krukiewicz, Corrosion behaviour of Fe-Mn-Si-Al austenitic steel in chloride solution, Journal of Achievements in Materials and Manufacturing Engineering 33/2 (2009) 159-165.
[24] S. Prowans, Physical metallurgy, PWN, Warsaw, 1988 (in Polish).
[25] R.A. Cottis, Stress corrosion cracking, Corrosion and Protection Centre, UMIST, Teddington, 1982.